Meningeal macrophages exhibit diverse calcium signaling at steady state and in response to aberrant cortical hyperexcitability in awake mice.

Simone Carneiro-Nascimento[1], Chao Wei[1], Anna Gutterman[1], Dan Levy[1,2*]

[1]Department of Anesthesia, Critical Care and Pain Medicine, Beth Israel Deaconess Medical Center, Harvard Medical School, Boston, United States

[2]Lead contact

*Correspondence: dlevy1@bidmc.harvard.edu

Abstract

The meninges, which envelop and protect the brain, host a large number of resident macrophages that play a crucial role in regulating homeostasis and neuroinflammation. Intracellular Ca^{2+} signaling mediates a variety of macrophage functions. While diverse, ontogeny, transcriptional profiles, and phenotypes of meningeal macrophages have been described, little is known about their spatiotemporal Ca^{2+} signal dynamics in healthy and diseased states. We used two-photon Ca^{2+} imaging in a novel reporter mouse line, combined with an event-based signaling analysis pipeline, to comprehensively characterize the Ca^{2+} activity of meningeal macrophages both at steady state and in response to cortical spreading depolarization (CSD) - a pathophysiological brain hyperexcitability event, implicated in migraine, traumatic brain injury, and stroke. In homeostatic meninges of behaving mice, perivascular macrophages exhibit several Ca^{2+} activity features, including event duration and signal frequency spectrum, distinct from those of interstitial non-perivascular macrophages. The Ca^{2+} activity of dural perivascular macrophages is uniquely coupled to behaviorally driven diameter fluctuation of their associated vessels. Most perivascular and non-perivascular meningeal macrophages display propagating intracellular Ca^{2+} activity. Both macrophage subtypes also exhibit synchronized intercellular Ca^{2+} elevations, likely driven by an external factor. In response to CSD, the majority of perivascular and non-perivascular meningeal macrophages show a persistent decrease in their Ca^{2+} activity. Smaller subsets of both macrophage subtypes display either acute or persistent increases in Ca^{2+} activity, with the latter response mediated by CGRP/RAMP1 signaling. Collectively, our results highlight a previously unknown diversity of meningeal macrophage Ca^{2+} signaling at steady-state and in response to an aberrant brain hyperexcitability event.

Introduction

Resident macrophages are key myeloid immunocytes that maintain homeostasis and play an important role in innate immune surveillance and defense across various peripheral tissues and organs [1-3]. The central nervous system also harbors a large subset of parenchymal macrophages, known as microglia, and several other distinct subsets of border-associated macrophages localized to the choroid plexus, perivascular spaces, and the meningeal compartments that cover, protect, and support the brain [4-8]. Recent studies demonstrated diverse ontogeny, transcriptomic profiles, and immune functions of macrophages in different meningeal areas at steady state [5,8-12] and neuropathological conditions [8,13-16].

Cytoplasmic calcium (Ca^{2+}) signaling underlies a wide variety of cellular homeostatic and inflammatory processes in macrophages [17-23]. In addition to intracellular Ca^{2+} elevation, distinct spatiotemporal dynamics, including oscillation patterns, intracellular propagations, and intercellular synchronization of Ca^{2+} signals, may regulate different macrophage functions during steady-state and pathophysiology [20-25]. Despite our increased understanding of the diversity of meningeal macrophages' molecular signatures and contribution to homeostasis and neuroinflammation, very little is known about their spatiotemporal Ca^{2+} signaling heterogeneity under both steady state and pathophysiological conditions.

To comprehensively characterize the Ca^{2+} activity of individual macrophages localized to the brain meninges, we combined intravital two-photon Ca^{2+} imaging in a novel reporter mouse line with an event-based signaling analysis pipeline. Our data reveal several distinct spatiotemporal Ca^{2+} activity features in perivascular and non-perivascular meningeal macrophages, including unique functional interactions between dural perivascular macrophages and behaviorally-driven dural vessels at steady state. Our data also reveal distinct patterns of meningeal macrophage Ca^{2+} activity changes in response to cortical spreading depolarization (CSD), a pathophysiological brain hyperexcitability event implicated in migraine, traumatic brain injury, and stroke, as well

as the contribution of CGRP receptor activation to CSD-evoked macrophage Ca^{2+} elevation, supporting their role in brain-to-meninges neuroimmune signaling.

Results

Characterizing macrophage Ca^{2+} signaling features in homeostatic brain meninges

Previous intravital imaging studies exploring the spatiotemporal dynamics of tissue-resident macrophages have primarily used CX3CR1-based mouse reporter strains [13,22,26,27]. However, other resident monocyte-derived cells are labeled in these reporter mice [28,29]. Moreover, brain microglia also express CX3CR1 [13,29-31], limiting the use of these reporter mice for resolving the spatiotemporal subcellular Ca^{2+} dynamics of macrophages localized to the thin meningeal layers covering the brain parenchyma. To systematically characterize meningeal macrophage Ca^{2+} activity *in vivo* and avoid contamination from Ca^{2+} signals arising from other resident monocyte-derived meningeal cells and superficial parenchymal microglia, we leveraged recent findings showing the expression of platelet factor 4 (Pf4) in meningeal macrophages but not in parenchymal microglia, meningeal monocytes or neutrophils [10,16,32], and generated transgenic reporter mice expressing the highly sensitive Ca^{2+} indicator GCaMP6s in $Pf4^{+}$ macrophages ($Pf4^{Cre}$:$GCaMP6s^{fl/wt}$). Notably, nearly 100% of meningeal macrophages are labelled in $PF4^{Cre}$-based reporter mice [32]. Although Pf4 is also expressed by megakaryocytes [33], these cells are absent in the brain meninges [5].

Anesthesia impacts intracellular Ca^{2+} signaling in brain macrophages and other non-excitable glial cells [34-36]. We therefore investigated subcellular Ca^{2+} activity of meningeal macrophages in awake, behaving mice. We imaged meningeal macrophages via a chronic cranial window implanted together with a restraining headpost over the intact dura mater overlying the posterior neocortex. After at least 7 days of recovery, mice were gradually habituated across multiple days to head restraint while free to run on a

wheel (**Figure 1b**). We tracked homeostatic Ca^{2+} transients of GCaMP6s-labeled meningeal macrophages using high-speed two-photon microscopy in 37 fields of view (FOVs) from 7 mice. We first corrected the imaging movies for locomotion-evoked meningeal translational shifts using rigid registration [37]. Movies were then processed using the AQuA2 data analysis platform [38], which implements an unbiased event-based approach to capture spatiotemporal Ca^{2+} event dynamics (**Figure 1C**). Based on spatial analysis, we assigned events (n=1361), with their corresponding calcium features, to a given macrophage, with data gathered from a total of 503 cells.

We characterized ongoing Ca^{2+} activity in two anatomically distinct macrophage populations: perivascular and interstitial non-perivascular (n=122; n=381, respectively, **Figure 2A and Video S1**). The vast majority of perivascular macrophages (93.4%, n=114) displaying ongoing Ca^{2+} activity were associated with vessels in the dural meningeal compartment. The two meningeal macrophage subpopulations exhibited several distinct Ca^{2+} activity features. While the total area of Ca^{2+} activity in the peri- and non-perivascular macrophages was similar (**Figure 2B**), the signal perimeter of perivascular macrophages was significantly higher (**Figure 2C**) and exhibited a more elongated shape (**Figures 2A, D**). The Ca^{2+} event duration in the perivascular macrophages was also longer compared to the non-perivascular subpopulation (**Figure 2F**). The peak Ca^{2+} activity level (Max $\Delta F/F_0$, **Figure 2E**) and event rate (**Figure 2G**), nonetheless, were similar in the two meningeal macrophage subpopulations.

Distinct Ca^{2+} signal frequency spectra may underlie different biological functions of macrophages [22]. We therefore analyzed meningeal macrophage Ca^{2+} signal waveforms by performing a multi-step signal processing and clustering analysis. We clustered cells based on two distinct patterns of Ca^{2+} activity. Cells in cluster 1 (n=40) exhibited a more noisy-like activity pattern characterized by multiple frequencies, while cells in Cluster 2 (n=463) displayed a single dominant frequency at 0.01 Hz (**Figure 3A**). To further explore these cellular signaling differences, we combined the clustering data with AQuA2-derived features and observed that macrophages in Cluster 1 showed a larger

event perimeter and lower circularity and peak magnitude compared to those in Cluster 2 (**Figures 3D-F**). Cluster 1 cells also had a lower signal-to-noise ratio compared to Cluster 2 cells (**Figure 3I**), but had differences in terms of event area, duration, or rate (Figures 3C, G, H). There was a significant association between cell cluster (1 vs. 2) and cell type, with Cluster 1 predominantly comprised of perivascular macrophages, and Cluster 2 including primarily non-perivascular macrophages (**Figure 3J**), further indicating that these two meningeal macrophage subpopulations have distinct Ca^{2+} signaling properties.

Intracellular Ca^{2+} signal propagation underlies diverse cellular functions and has been recently identified in microphages in vitro [21] and skin resident macrophages in vivo [39]. By assessing the Ca^{2+} signal propagation maps of each event within a determined cell, we identified two distinct patterns of activity: propagating events in which Ca^{2+} signals traveled throughout the entire cell, and stationary events (**Figure 4A**). Propagating events had varied signal source regions and directionality. Most macrophages (perivascular, 94.3%, n=115, non-perivascular, 86.9%, n=331) exhibited only propagating events, while a small minority of cells displayed a mix of propagating and stationary events or exclusively stationary activity events (**Figure 4B**).

Macrophage intercellular communication, including synchronized activity, potentially across connected macrophage networks, has been implicated in maintaining tissue homeostasis and immune function [18,21,40,41]. To investigate meningeal macrophage intercellular interactions, we characterized spatiotemporal relationships between Ca^{2+} events in distinct cells within each FOV. We compared temporal factors, including the relative onset latency ($t0_A – t0_B$) between different macrophages and the duration of the first occurring event ($t1_A – t0_A$) (**Figure 4C**). We also compared the distances between macrophage pairs exhibiting concurrent events and the number of synchronous events (**Figure 4D**). Finally, we calculated the proportion of perivascular and non-perivascular macrophages exhibiting synchronous Ca^{2+} events. Across all FOVs, nearly half of the macrophages (49.3%) exhibited synchronous Ca^{2+} activity, involving cells at a wide range of distances (**Figure 4E**), suggesting that spatial proximity does not influence

event synchronicity. Interestingly, there was poor correlation between the distance of cell pairs exhibiting synchronous events and their timing (**Figure 4F**), suggesting that an external factor, rather than intercellular coordinated networked activity, mediates this intercellular signaling. When comparing synchronous activity among peri- and non-perivascular macrophages, most cells exhibited mixed interactions between the same and different subtypes (**Figure 4G**).

Dural perivascular macrophage Ca^{2+} activity is tuned to behaviorally-driven dural vasomotion

Brain border macrophages in the leptomeninges and related parenchymal perivascular spaces regulate pial arterial vasomotion indirectly by affecting vessel stiffness [6]. Yet, interaction between vascular-associated macrophages residing in the dura mater, the outermost meningeal layer, and dural vasomotion remains unknown. As we detected very few perivascular leptomeningeal macrophages with ongoing Ca^{2+} activity, we focused on the functional interaction between dural vessels and their associated perivascular macrophages. We employed a Generalized Linear Model (GLM) approach to investigate the relationship between dural perivascular macrophage Ca^{2+} signals and behaviorally driven dural vessel dynamics (**Figure 5A**). Dural arteries constrict during locomotion, while pial arteries dilate [42]. We analyzed the locomotion-associated responses of 86 meningeal vessels (32 FOVs from 5 mice) and identified a subset (22%, n=19), whereby the diameter changes were well fit by a GLM using the locomotion state as a predictor. Of these, we identified 74% (n=14) as dural vessels based on their GLM's negative coefficients consistent with constriction (**Figures 5B, C**). Next, we fit the Ca^{2+} signal observed in perivascular macrophages associated with these dural vessels (n=35) to a GLM using the diameter changes as a predictor variable. Overall, the Ca^{2+} activity of 83% (n=29) of these dural macrophages was well predicted by the model (average deviance explained across all well-fit macrophages: 0.43 +/- 0.15, mean +/- SD). Analysis of the macrophage-vascular models' beta coefficients revealed two distinct interactions. About half of the macrophages (55%, n=13) exhibited negative coefficients (i.e., increase and decrease in Ca^{2+} activity

associated with dural vasoconstriction and recovery, respectively, **Figure 5B, D**). The remaining macrophages (45%, n=16) exhibited positive coefficients (i.e., decrease and increase in Ca^{2+} activity in response to dural constriction and recovery, respectively; **Figure 5B, E**). The coefficients for increased and decreased macrophage Ca^{2+} activity peaked near zero delay relative to the vasoconstriction and were not statistically different (**Figures 5D-E, H**). These data provide evidence that dural perivascular macrophages are functionally coupled to dural vasomotion, either responding to or mediating such behaviorally-driven vascular response.

An acute migraine-related aberrant brain excitability event drives diverse Ca^{2+} responses in meningeal macrophages

In anesthetized mice, a small subset of meningeal macrophages undergoes morphological changes resembling an inflammatory-state in a model of cortical spreading depolarization (CSD), a brain hyperexcitability event linked to migraine, traumatic brain injury, and stroke [43-45]. Given the direct anatomical and functional connection between the brain and meninges [11,46] and the involvement of intracellular Ca^{2+} influx in macrophage inflammatory activation [47], we asked whether, in the wake of CSD, brain-to-meninges signaling drives intracellular Ca^{2+} elevations in meningeal macrophages. We therefore triggered a single CSD episode in the frontal cortex [48,49] and characterized the related changes in meningeal macrophage Ca^{2+} dynamics. In each experiment, we verified CSD induction based on the associated acute meningeal deformation and/or pial vasoconstriction observed in awake animals ([49] and **Video S2**). We studied CSD-related Ca^{2+} activity changes in 249 macrophages (perivascular, n=64; non-perivascular, n=185; 13 FOVs from 10 mice). In each cell, we compared Ca^{2+} calcium event rates during the passing of the CSD wave (1 min) and the PostCSD period (30 min) to baseline (PreCSD, 30 min) to assess acute and persistent Ca^{2+} responses, respectively. We characterized cells as exhibiting persistently increased (event rate > 2× PreCSD), decreased (event rate < 0.5× PreCSD), or unchanged responses. Given the low activity rate observed under steady-state and the likelihood that no spontaneous Ca^{2+} response occurs during the brief period of the CSD event, we

considered cells only as acutely activated or exhibiting unchanged Ca^{2+} response. CSD evoked both acute and persistent Ca^{2+} activity changes in (**Figures 6 A-E and Video S2**). While smaller subsets of meningeal macrophages exhibited acute (21.3%, n=52) and/or persistent increase (22.1%, 55/249) in their Ca^{2+} activity, the majority of cells (58.6%, n=146) exhibited a persistent decrease. An acute increase was observed more often in peri- vs non-perivascular macrophages (perivascular, n = 32.8%, n=21; non-perivascular, n = 17.3%, n=32, **Figure 6F**). Persistent increases or decreases in Ca^{2+} activity were observed similarly in peri- and non-perivascular macrophages (increases; perivascular, 28.2%; n=18; non-perivascular, 18.4%, n=34; decrease perivascular, 50.0%, n=32; non-perivascular, 61.6%, n=113, **Figure 6G**). The macrophages' propensity to develop a persistent Ca^{2+} increase was unrelated to their acute response (**Figure 6H**), suggesting that the mechanisms underlying these two temporal responses are distinct. However, cells showing no acute activation were more likely to display decreased calcium activation post-CSD (**Figure 6H**). Finally, we observed that macrophages exhibiting a persistent increase in Ca^{2+} activity had a lower baseline activity when compared to cells showing a persistent (**Figure 6 I**), suggesting that this post-CSD response is influenced by the macrophages' basal response activity.

CGRP-RAMP1 mediates CSD-evoked persistent increase in meningeal macrophage Ca^{2+} activity

Many meningeal macrophages are localized near nociceptor axons [16]. In the wake of CSD, cortex-to-meninges signaling enhances the responsiveness of meningeal nociceptive neurons and can drive the release of the neuropeptide CGRP from their peripheral nerve endings [48-50]. CGRP-expressing nociceptive neurons regulate tissue immunity, including meningeal macrophage function, via the CGRP-RAMP1 neuroimmune axis [16,51]. We therefore asked whether the CSD-related meningeal macrophage Ca^{2+} changes we observed involve CGRP-RAMP1 signaling. We pretreated mice with the RAMP1 antagonist BIBN4096 and then imaged meningeal macrophage Ca^{2+} activity (42 cells; perivascular, n=14; non-perivascular, n=28, from 3 FOVs in 3 mice) before and after CSD. As expected, RAMP1 blockade did not affect

CSD triggering [52]. When compared to control saline treatment, RAMP1 blockade also did not reduce basal macrophage Ca^{2+} activity (**Figure 7B**). Blocking CGRP-RAMP1 signaling neither affected the incidence of acute increases in Ca^{2+} activity (**Figures 7A, C**) nor the magnitude of that response (**Figure 7D**). RAMP1 antagonism, however, inhibited the CSD-evoked persistent increase in the macrophage's Ca^{2+} activity, without affecting the incidence of the persistent decrease (**Figure 7E**). The data suggest that in the wake of CSD, the CGRP-RAMP1 axis, likely involving a peripheral neuroimmune signaling, is responsible for the prolonged enhancement of Ca^{2+} signaling in a subset of meningeal macrophages, which could potentially mediate their pro-inflammatory response.

Discussion

Macrophages localized to the brain meninges are essential for maintaining brain homeostasis, regulating central nervous system immune surveillance, and mediating neuroimmune response under pathological conditions [12,14,16,53-55]. Macrophages rely on Ca^{2+} signaling to mediate many of their functions [17-23]. Here, using two-photon microscopy, we characterized for the first time the Ca^{2+} activity of meningeal macrophages in awake, behaving $Pf4^{Cre}$:$GCaMP6s^{fl/wt}$ reporter mice under state-state and migraine-like conditions. We describe two subpopulations of macrophages, perivascular and non-perivascular, that exhibit several distinct Ca^{2+} signal properties in homeostatic meninges. We further demonstrate Ca^{2+} activity in dural perivascular macrophages tuned to behaviourally-driven dural vasomotion. We further identified diverse Ca^{2+} responses of meningeal macrophages associated with an aberrant cortical hyperexcitability event, related to migraine, traumatic brain injury, and stroke, and demonstrate the contribution of the CGRP/RAMP1 axis in mediating persistent Ca^{2+} elevations.

The exact link between the distinct Ca^{2+} signal properties of meningeal macrophage subsets observed herein and their homeostatic function remains to be established. The lower event magnitude and noisier signal observed in dural perivascular macrophages

may reflect functional interactions with the pulsation dynamics of dural vessels [42]. Indeed, by combining vascular and macrophage Ca^{2+} imaging, we have uncovered a tight temporal association between the diameter fluctuations of the dural vessels and the Ca^{2+} signal of their associated macrophages in awake, locomoting mice. Direct vascular-macrophage coupling may underlie this interaction, involving macrophages sensing vascular-related mechanical changes via Piezo1 signaling [56]. Functional vascular-macrophage interaction may also involve mural cells as intermediators [54,57]. Studying whether macrophage Ca^{2+} signaling regulates dural vasomotion will require an experimental approach that has yet to be developed, allowing for the selective manipulation of dural perivascular macrophages. The paucity of ongoing Ca^{2+} activity in perivascular macrophages situated in the leptomeninges supports recent findings that subdural perivascular macrophages indirectly affect pial and brain vasomotion by controlling extracellular matrix (ECM) remodeling [6].

Intracellular Ca^{2+} signal propagation has been observed in various non-excitable cells, such as astrocytes [58]. We show that the majority of meningeal macrophages, including peri- and non-perivascular, exhibit Intracellular Ca^{2+} signal propagation that travels throughout the entire cell, suggesting microdomain intracellular Ca^{2+} signal elevation, following release from internal stores. By characterizing the spatiotemporal relationships between Ca^{2+} signals in distinct cells, we also observed synchronous events that were independent of spatial proximity, suggesting that synchronous Ca^{2+} responses are not driven by intercellular communication but rather by an external signal. Interestingly, synchronized events involved both peri- and non-perivascular macrophages, despite having distinct Ca^{2+} elevation features, suggesting that these meningeal macrophage subtypes similarly sense external signals directly or indirectly.

Cortex-to-meninges signaling involves a relatively slow flow of molecules in the cerebrospinal fluid reaching the subarachnoid space and advancing across the arachnoid barrier into the dura mater [11,46]. The rapid Ca^{2+} elevation we observed in a subset of extrasinusoidal perivascular dural macrophages in the wake of CSD suggests a faster transfer of chemical signals from the cortex across all meningeal layers [44].

Nevertheless, we cannot exclude a mechanically driven macrophage response to the acute meningeal deformation produced by the neuronal and glial swelling and shrinkage of the cortical extracellular space during CSD [49,59,60]. The prolonged increase in Ca^{2+} signal we identified in a small subset of macrophages post-CSD could underlie their proinflammatory-like morphological change [45,47]. We also identified CGRP/RAMP1 signaling as a putative neuroimmune mechanism responsible for this macrophage Ca^{2+} response, likely via the activation of their CGRP receptors [16]. Whether the small subset of meningeal macrophages featuring CGRP-mediated increased Ca^{2+} signaling represents a cellular subset that assumes either a protective role [61,62] or a proinflammatory, destructive function [63] remains to be elucidated. Intriguingly, we identified a persistent decrease in Ca^{2+} activity post-CSD, not involving a CGRP/RAMP1 signaling, as the most prevalent response, potentially involving a distinct damping effect of meningeal immunity driven by a hyperexcitable brain.

In summary, we provide a detailed characterization of the homeostatic Ca^{2+} activity of meningeal macrophages, expanding our knowledge of the biological diversity of brain border macrophages. The coupling of dural perivascular macrophage Ca^{2+} signals and dural vasomotion may represent a unique homeostatic functional dural macrophage-vascular unit. The diversity of meningeal macrophage Ca^{2+} responses to CSD further highlights the complexity of brain-to-meninges signaling and meningeal macrophage function in neurological disorders such as migraine. Our study also provides essential genetic and data analysis tools to further understand the molecular signaling underlying macrophage function at steady state and neuropathological conditions.

Acknowledgements

The study was supported by NIH grants: R21NS130561; R01NS115972 and R01NS133625 to D.L.

Author contributions

D.L. conceived the project. S.C-N and D.L. wrote the manuscript. S.C-N performed two-photon imaging and data analysis with help from D.L. S.C-N, C.W., and A.G. performed surgeries.

Methods

RESOURCE AVAILABILITY

Lead contact

Requests for information or resources should be directed to the lead contact, Dan Levy (dlevy1@bidmc.harvard.edu)

Material availability

This study did not generate any new reagents.

Data and code availability

The code used for movie processing is available at: https://github.com/levylabheadache/MovieProcessing/tree/SCN; Code for locomotion analysis is available at: https://github.com/levylabheadache/Locomotion/tree/SCN ; Code for post Aqua2-processing is available at: https://github.com/levylabheadache/Aqua2Processing; Code for vascular segmentation is available at: https://github.com/levylabheadache/Vasculature/tree/SCN ; Code for GLM is available at: https://github.com/levylabheadache/GeneralLinearModel_Macrophages

Any additional information required to reanalyze the data reported in this paper is available from the lead contact upon request.

DECLARATION OF GENERATIVE AI AND AI-ASSISTED TECHNOLOGIES IN THE WRITING PROCESS

During the preparation of this work, the authors used ChatGPT in order to check for grammar and style. After using this tool/service, the authors reviewed and edited the content as needed and take full responsibility for the content of the published article.

METHODS DETAILS

Experimental model and study participants

All experiments were conducted on adult $Pf4^{Cre}$:$GCaMP6s^{fl/wt}$ Ca^{2+} reporter mice (8-17 weeks) (9 males, 5 females). Mice were generated by crossing $Pf4^{Cre}$ (C57BL/6-Tg (Pf4-icre) Q3Rsko/J, Jackson laboratory, Strain #008535) mice with $GCaMP6s^{fl/fl}$ (B6.Cg-$Igs7^{tm162.1(tetO\text{-}GCaMP6s,CAG\text{-}tTA2)Hze}$/J, Jackson laboratory, Strain #031562) mice. Transgenic animals were genotyped by Transnetyx Inc. Experimental procedures were approved by the Beth Israel Deaconess Medical Center Institutional Animal Care and Use Committee.

Surgical procedures

Animals were anesthetized using isoflurane in 100% O_2 (induction: 3%; maintenance: 1.5-2%) and placed on a heating pad with a rectal probe attached to a stereotaxic frame to monitor animal body temperature during surgery. Animals received dexamethasone (8 mg/kg, i.p.) and Meloxicam SR (4 mg/kg, s.c.) to reduce inflammation and improve surgical outcomes. An eye ointment was used to prevent ocular drying. Mice were implanted with a titanium headpost and a 3 mm glass cranial window (1.5 mm lateral and 2 mm posterior to Bregma) over an intact dura covering the left posterior neocortex [49]. Immediately after surgery, the mouse cage was placed on a water-circulating heating pad for faster recovery. Animals were then single-housed with access to a running wheel and a hut and allowed to recover for at least one week.

Wheel running acclimation

After the cranial window surgery, mice were allowed to recover for at least a week. To reduce stress associated with head-fixation during imaging and habituate to wheel

running, the mice received multiple training sessions (10 min to 1 h over 3–4 days). In each session, the mouse was placed on a 3D printed running wheel, with its headpost attached to two clamps, and allowed to locomote freely.

Two-photon Ca^{2+} imaging

Awake-behaving mice were head-fixed to the running wheel by its headpost (**Figure 1**). We used a two-photon microscope (Neurolabware) with a Nikon 16X, 0.8 NA objective to acquire images at 15.5 Hz with digital zoom set at 4X (312 x 212 μm^2 FOV). A MaiTai laser, set to 920 nm with 25–40 mW power, was used to excite fluorescence. The Scanbox package for MATLAB (Neurolabware) was used to control the microscope and acquire images and wheel running data. To image the meningeal vasculature, mice were administered 70kDa TRITC-Dextran tracer (50 mg/kg, i.v.; Sigma-Aldrich).

Behavioral tracking during two-photon imaging

We recorded running speed in MATLAB using a custom-made encoder (Arduino) coupled to the 3D-printed running wheel. See below for details of analyses of behavioral variables.

Induction of CSD and pharmacological treatment

For CSD induction, a 1 mm burr hole was drilled at the frontal bone (1.5 mm anterior to the cranial window) to allow access to the brain cortical surface. A small amount of silicone elastomer (Kwik-Cast, WPI) was placed to cover the burr hole opening, and the animal was left to recover for at least one week. On the experimental day, 30 minutes before baseline recording, mice were pretreated with the CGRP RAMP1 receptor antagonist BIBN4096 (1 mg/kg, i.p., Tocris [50]) or 0.9% saline. CSD was induced using a brief 2-second cortical pinprick [49]. CSD induction was confirmed by the identification of a short-lasting meningeal deformation and/or transient pial constriction [49].

QUANTIFICATION AND STATISTICAL ANALYSIS

Two-photon imaging movie processing

Rigid registration using the discrete Fourier transform was used to correct translation changes due to brain motion during locomotion. Movies were then downsampled to 1.03 Hz. Locomotion signals were detected as described [37]. All image processing and locomotion signal extraction were performed in MATLAB 2021b (Mathworks).

Ca^{2+} signal detection pipeline

For detecting macrophage Ca^{2+} signals, we used the Activity Quantification and Analysis (AQuA2) platform [38] that implements an event-based approach with advanced machine learning techniques for temporal and spatial segmentation of Ca^{2+} fluorescence events, capturing event dynamics beyond traditional ROI-based approaches. The following user-defined parameters were input: 0.49 µm/pixel spatial resolution, 1.03 Hz temporal resolution, 1-second minimal event duration detection; window of event size between 25% (125 μm^2/ 523 pixels) and 150% (750 μm^2/ 3140 pixels). Every event and cell identified was followed by a manual visual check, and each cell was labeled as perivascular or non-perivascular according to its location relative to vessels. Morphological features (area, perimeter, circularity) and spatiotemporal aspects of the calcium signals (i.e., dF/F_0 dynamics, frequency, amplitude, duration) were used to analyze cell-specific characteristics and Ca^{2+} activity profiles. We employed the AQuA2 automatically-generated propagation maps [38] to characterize intracellular Ca^{2+} propagation. Intercellular calcium activity was evaluated by analyzing temporally co-occurring events (synchronized event pairs), as well as their corresponding spatial localization in the FOV. All post-processing of AQuA2-generated data was performed using MATLAB 2021b (Mathworks).

Clustering of Ca^{2+} dynamics

A Savitzky-Golay filter was used to detrend and smooth Ca^{2+} activity traces. Polynomial order and frame size were optimized for each cell by selecting the combination of parameters that yielded a better signal-to-noise ratio. From the filtered signals, we extracted the dominant frequency using Fast Fourier Transform, and peak counts using

minimum peak prominence (threshold of 10% signal amplitude range). The optimal number of clusters was determined using the Elbow method, after which k-means clustering was applied to group cells based on their signal characteristics.

Analysis of CSD-related changes in macrophage Ca^{2+} Activity

For analyzing of the effects of CSD on macrophages' Ca^{2+} dynamics, each cell activity was divided into three phases: 'PreCSD' (minutes 0 – 30), 'DuringCSD' (minutes 30 – 31), and 'PostCSD' (minutes 31 – 61). Ca^{2+} event rate during CSD and PostCSD was compared against that of the PreCSD baseline for evaluation of acute and persistent calcium responses, respectively. Ca^{2+} responses were categorized as increased (event rate > 2x PreCSD), decreased (event rate < 0.5x PreCSD), or unchanged.

Analysis of locomotion

Running speed traces were extracted (cm/s) from the encoder attached to the wheel. To infer the locomotion state, we first concatenated all velocity signals obtained from a given mouse across all experiments and trained a two-state Hidden Markov Model using the MATLAB function 'hmmtrain'. Then, the locomotion state was inferred for each individual imaging run by applying the MATLAB function 'hmmviterbi' with the model trained on the concatenated data. Locomotion bouts were defined as periods when the locomotion state was sustained for at least two seconds.

Vascular signals

Changes in vascular diameter were calculated by first generating a maximum intensity projection of the red channel and drawing polygons (ROIs) around each vessel. Subsequently, for each frame, pixels inside each ROI were extracted, and a Radon transform was applied to get a 1D vessel profile. Radon transform of the first frame was used as a reference to normalize the results of all subsequent frames, resulting in a time series of normalized diameter traces.

***General linear models* (GLM)**

We investigate the functional interaction between dural perivascular macrophage Ca^{2+} activity and dural vasomotion by fitting a Gaussian GLMs using the GLMnet package (MATLAB 2021b), with elastic net regularization (α = 0.01) and ten-fold cross-validation. We employed a two-step modeling. The first model was used to identify dural vessels by evaluating the correlation of vessel diameter changes to locomotion state, classifying dural or pial vessels according to their vasoconstriction and vasodilation dynamics, respectively [42]. The second modeling step evaluated the correlation between perivascular dural Ca^{2+} activity signals and dural vessel diameter changes. All signals were downsampled to 1.03 Hz to match the frame rate used when extracting fluorescence Ca^{2+} signals in AQuA2. To allow potential anticipatory or delayed responses of diameter-to-locomotion or Ca^{2+} fluorescence-to-diameter, the time interval used to analyze the response to the predictor was set from -60 s to +60 s. The GLM was trained on 75% of the data, and all predictions and model performances reported are from the remaining 25% testing set. A threshold of 0.1 goodness-of-fit deviance explained was set. For each predictor temporal shift, a response coefficient was generated. Centroid delay between predictor and response was calculated, weighted by the absolute value of the coefficient (i.e., center-of-mass, COM).

Statistical analysis

All statistical analysis was performed using GraphPad Prism 10.4 and MATLAB 2021b. Data were analyzed using a Wilcoxon matched-pairs signed rank sum test or a Mann-Whitney U-test. Distribution of categorical data was analyzed using the Chi-square or Fisher's exact test. P-values are indicated as follows: *p< 0.05, **p<0.01, ***p<0.001, ****p<0.0001.

KEY RESOURCES TABLE

REAGENT OR RESOURCE	SOURCE	IDENTIFIER
Chemicals		
75-85kDa TRITC-Dextran	Sigma-Aldrich	Cat #T1162
BIBN4096	Tocris	Cat #4561

Animal Models Organism/Strains		
Pf4^{cre} (C57BL/6-Tg (Pf4-icre) Q3Rsko/J	The Jackson Laboratory	JAX Strain #008535
GCaMP6s^{fl} (B6.Cg-Igs7$^{tm162.1(tetO-GCaMP6s,CAG-tTA2)Hze}$/J	The Jackson Laboratory	JAX Strain #031562
Software and algorithms		
Matlab 2021/2202b	Mathworks	https://www.mathworks .com/products/matlab; RRID: SCR_001622
AQUA2	Mi et al. 2025	https://github.com/yu-lab-vt/AQuA2
GraphPad Prism 10.4.1	GraphPad	https://www.graphpad.com RRID:SCR_002798
MATLAB code for movie processing	Blaeser et al., 2022	levylabheadache/MovieProcessing
MATLAB code for locomotion analysis	Blaeser et al., 2022	levylabheadache/Locomotion
MATLAB code for post-AQuA2 processing	This paper	levylabheadache/Aqua2Processing
MATLAB code for vasculature segmentation	This paper	levylabheadache/Vasculature
MATLAB code for GLM	Blaeser et al., 2022	levylabheadache/GeneralLinearModel
Other		
Two-photon microscope	Neurolabware	http://Neurolabware.com
Mai Tai laser	Spectra-Physics	Mai Tai HP
16X, 0.8 NA objective	Nikon/Thorlabs	N16XLWD-PF

References

1. Okabe, Y., and Medzhitov, R. (2016). Tissue biology perspective on macrophages. Nat Immunol *17*, 9-17. 10.1038/ni.3320.

2. Guilliams, M., Thierry, G.R., Bonnardel, J., and Bajenoff, M. (2020). Establishment and Maintenance of the Macrophage Niche. Immunity *52*, 434-451. 10.1016/j.immuni.2020.02.015.
3. Mass, E., Nimmerjahn, F., Kierdorf, K., and Schlitzer, A. (2023). Tissue-specific macrophages: how they develop and choreograph tissue biology. Nature reviews *23*, 563-579. 10.1038/s41577-023-00848-y.
4. Kierdorf, K., Masuda, T., Jordao, M.J.C., and Prinz, M. (2019). Macrophages at CNS interfaces: ontogeny and function in health and disease. Nat Rev Neurosci *20*, 547-562. 10.1038/s41583-019-0201-x.
5. Rustenhoven, J., Drieu, A., Mamuladze, T., de Lima, K.A., Dykstra, T., Wall, M., Papadopoulos, Z., Kanamori, M., Salvador, A.F., Baker, W., et al. (2021). Functional characterization of the dural sinuses as a neuroimmune interface. Cell *184*, 1000-1016 e1027. 10.1016/j.cell.2020.12.040.
6. Drieu, A., Du, S., Storck, S.E., Rustenhoven, J., Papadopoulos, Z., Dykstra, T., Zhong, F., Kim, K., Blackburn, S., Mamuladze, T., et al. (2022). Parenchymal border macrophages regulate the flow dynamics of the cerebrospinal fluid. Nature *611*, 585-593. 10.1038/s41586-022-05397-3.
7. Masuda, T., Amann, L., Monaco, G., Sankowski, R., Staszewski, O., Krueger, M., Del Gaudio, F., He, L., Paterson, N., Nent, E., et al. (2022). Specification of CNS macrophage subsets occurs postnatally in defined niches. Nature *604*, 740-748. 10.1038/s41586-022-04596-2.
8. Amann, L., Fell, A., Monaco, G., Sankowski, R., Wu, H.Z.Q., Jordao, M.J.C., Borst, K., Fliegauf, M., Masuda, T., Ardura-Fabregat, A., et al. (2024). Extrasinusoidal macrophages are a distinct subset of immunologically active dural macrophages. Sci Immunol *9*, eadh1129. 10.1126/sciimmunol.adh1129.
9. Mrdjen, D., Pavlovic, A., Hartmann, F.J., Schreiner, B., Utz, S.G., Leung, B.P., Lelios, I., Heppner, F.L., Kipnis, J., Merkler, D., et al. (2018). High-Dimensional Single-Cell Mapping of Central Nervous System Immune Cells Reveals Distinct Myeloid Subsets in Health, Aging, and Disease. Immunity *48*, 380-395 e386. 10.1016/j.immuni.2018.01.011.
10. Van Hove, H., Martens, L., Scheyltjens, I., De Vlaminck, K., Pombo Antunes, A.R., De Prijck, S., Vandamme, N., De Schepper, S., Van Isterdael, G., Scott, C.L., et al. (2019). A single-cell atlas of mouse brain macrophages reveals unique transcriptional identities shaped by ontogeny and tissue environment. Nat Neurosci *22*, 1021-1035. 10.1038/s41593-019-0393-4.
11. Smyth, L.C.D., Xu, D., Okar, S.V., Dykstra, T., Rustenhoven, J., Papadopoulos, Z., Bhasiin, K., Kim, M.W., Drieu, A., Mamuladze, T., et al. (2024). Identification of direct connections between the dura and the brain. Nature *627*, 165-173. 10.1038/s41586-023-06993-7.
12. Vara-Perez, M., and Movahedi, K. (2025). Border-associated macrophages as gatekeepers of brain homeostasis and immunity. Immunity *58*, 1085-1100. 10.1016/j.immuni.2025.04.005.
13. Rua, R., Lee, J.Y., Silva, A.B., Swafford, I.S., Maric, D., Johnson, K.R., and McGavern, D.B. (2019). Infection drives meningeal engraftment by inflammatory monocytes that impairs CNS immunity. Nat Immunol *20*, 407-419. 10.1038/s41590-019-0344-y.

14. Rebejac, J., Eme-Scolan, E., Arnaud Paroutaud, L., Kharbouche, S., Teleman, M., Spinelli, L., Gallo, E., Roussel-Queval, A., Zarubica, A., Sansoni, A., et al. (2022). Meningeal macrophages protect against viral neuroinfection. Immunity *55*, 2103-2117 e2110. 10.1016/j.immuni.2022.10.005.
15. De Vlaminck, K., Van Hove, H., Kancheva, D., Scheyltjens, I., Pombo Antunes, A.R., Bastos, J., Vara-Perez, M., Ali, L., Mampay, M., Deneyer, L., et al. (2022). Differential plasticity and fate of brain-resident and recruited macrophages during the onset and resolution of neuroinflammation. Immunity *55*, 2085-2102 e2089. 10.1016/j.immuni.2022.09.005.
16. Pinho-Ribeiro, F.A., Deng, L., Neel, D.V., Erdogan, O., Basu, H., Yang, D., Choi, S., Walker, A.J., Carneiro-Nascimento, S., He, K., et al. (2023). Bacteria hijack a meningeal neuroimmune axis to facilitate brain invasion. Nature *615*, 472-481. 10.1038/s41586-023-05753-x.
17. Desai, B.N., and Leitinger, N. (2014). Purinergic and calcium signaling in macrophage function and plasticity. Front Immunol *5*, 580. 10.3389/fimmu.2014.00580.
18. Zumerle, S., Cali, B., Munari, F., Angioni, R., Di Virgilio, F., Molon, B., and Viola, A. (2019). Intercellular Calcium Signaling Induced by ATP Potentiates Macrophage Phagocytosis. Cell Rep *27*, 1-10 e14. 10.1016/j.celrep.2019.03.011.
19. Seegren, P.V., Downs, T.K., Stremska, M.E., Harper, L.R., Cao, R., Olson, R.J., Upchurch, C.M., Doyle, C.A., Kennedy, J., Stipes, E.L., et al. (2020). Mitochondrial Ca(2+) Signaling Is an Electrometabolic Switch to Fuel Phagosome Killing. Cell Rep *33*, 108411. 10.1016/j.celrep.2020.108411.
20. Nascimento Da Conceicao, V., Sun, Y., Ramachandran, K., Chauhan, A., Raveendran, A., Venkatesan, M., DeKumar, B., Maity, S., Vishnu, N., Kotsakis, G.A., et al. (2021). Resolving macrophage polarization through distinct Ca(2+) entry channel that maintains intracellular signaling and mitochondrial bioenergetics. iScience *24*, 103339. 10.1016/j.isci.2021.103339.
21. Taghdiri, N., Calcagno, D.M., Fu, Z., Huang, K., Kohler, R.H., Weissleder, R., Coleman, T.P., and King, K.R. (2021). Macrophage calcium reporter mice reveal immune cell communication in vitro and in vivo. Cell Rep Methods *1*. 10.1016/j.crmeth.2021.100132.
22. Mehari, F.T., Miller, M., Pick, R., Bader, A., Pekayvaz, K., Napoli, M., Uhl, B., Reichel, C.A., Sperandio, M., Walzog, B., et al. (2022). Intravital calcium imaging in myeloid leukocytes identifies calcium frequency spectra as indicators of functional states. Sci Signal *15*, eabe6909. 10.1126/scisignal.abe6909.
23. Seegren, P.V., Harper, L.R., Downs, T.K., Zhao, X.Y., Viswanathan, S.B., Stremska, M.E., Olson, R.J., Kennedy, J., Ewald, S.E., Kumar, P., and Desai, B.N. (2023). Reduced mitochondrial calcium uptake in macrophages is a major driver of inflammaging. Nat Aging *3*, 796-812. 10.1038/s43587-023-00436-8.
24. Vaeth, M., Zee, I., Concepcion, A.R., Maus, M., Shaw, P., Portal-Celhay, C., Zahra, A., Kozhaya, L., Weidinger, C., Philips, J., et al. (2015). Ca2+ Signaling but Not Store-Operated Ca2+ Entry Is Required for the Function of Macrophages and Dendritic Cells. J Immunol *195*, 1202-1217. 10.4049/jimmunol.1403013.

25. Schappe, M.S., Stremska, M.E., Busey, G.W., Downs, T.K., Seegren, P.V., Mendu, S.K., Flegal, Z., Doyle, C.A., Stipes, E.J., and Desai, B.N. (2022). Efferocytosis requires periphagosomal Ca(2+)-signaling and TRPM7-mediated electrical activity. Nat Commun *13*, 3230. 10.1038/s41467-022-30959-4.
26. Ren, X., Manzanares, L.D., Piccolo, E.B., Urbanczyk, J.M., Sullivan, D.P., Yalom, L.K., Bui, T.M., Lantz, C., Najem, H., Dulai, P.S., et al. (2023). Macrophage-endothelial cell crosstalk orchestrates neutrophil recruitment in inflamed mucosa. J Clin Invest *133*. 10.1172/JCI170733.
27. Ishikawa-Ankerhold, H., Busch, B., Bader, A., Maier-Begandt, D., Dionisio, F., Namineni, S., Vladymyrov, M., Harrison, U., van den Heuvel, D., Tomas, L., et al. (2024). Novel multiphoton intravital imaging enables real-time study of Helicobacter pylori interaction with neutrophils and macrophages in the mouse stomach. PLoS Pathog *20*, e1012580. 10.1371/journal.ppat.1012580.
28. Chinnery, H.R., Ruitenberg, M.J., and McMenamin, P.G. (2010). Novel characterization of monocyte-derived cell populations in the meninges and choroid plexus and their rates of replenishment in bone marrow chimeric mice. J Neuropathol Exp Neurol *69*, 896-909. 10.1097/NEN.0b013e3181edbc1a.
29. Jung, S., Aliberti, J., Graemmel, P., Sunshine, M.J., Kreutzberg, G.W., Sher, A., and Littman, D.R. (2000). Analysis of fractalkine receptor CX(3)CR1 function by targeted deletion and green fluorescent protein reporter gene insertion. Mol Cell Biol *20*, 4106-4114. 10.1128/MCB.20.11.4106-4114.2000.
30. Roth, T.L., Nayak, D., Atanasijevic, T., Koretsky, A.P., Latour, L.L., and McGavern, D.B. (2014). Transcranial amelioration of inflammation and cell death after brain injury. Nature *505*, 223-228. 10.1038/nature12808.
31. Liu, Y.U., Ying, Y., Li, Y., Eyo, U.B., Chen, T., Zheng, J., Umpierre, A.D., Zhu, J., Bosco, D.B., Dong, H., and Wu, L.J. (2019). Neuronal network activity controls microglial process surveillance in awake mice via norepinephrine signaling. Nat Neurosci *22*, 1771-1781. 10.1038/s41593-019-0511-3.
32. McKinsey, G.L., Lizama, C.O., Keown-Lang, A.E., Niu, A., Santander, N., Larpthaveesarp, A., Chee, E., Gonzalez, F.F., and Arnold, T.D. (2020). A new genetic strategy for targeting microglia in development and disease. Elife *9*. 10.7554/eLife.54590.
33. Tiedt, R., Schomber, T., Hao-Shen, H., and Skoda, R.C. (2007). Pf4-Cre transgenic mice allow the generation of lineage-restricted gene knockouts for studying megakaryocyte and platelet function in vivo. Blood *109*, 1503-1506. 10.1182/blood-2006-04-020362.
34. Umpierre, A.D., Bystrom, L.L., Ying, Y., Liu, Y.U., Worrell, G., and Wu, L.J. (2020). Microglial calcium signaling is attuned to neuronal activity in awake mice. Elife *9*. 10.7554/eLife.56502.
35. Thrane, A.S., Rangroo Thrane, V., Zeppenfeld, D., Lou, N., Xu, Q., Nagelhus, E.A., and Nedergaard, M. (2012). General anesthesia selectively disrupts astrocyte calcium signaling in the awake mouse cortex. Proc Natl Acad Sci U S A *109*, 18974-18979. 10.1073/pnas.1209448109.
36. Zhou, H., Neudecker, V., Perez-Zoghbi, J.F., Brambrink, A.M., and Yang, G. (2024). Age-dependent cerebral vasodilation induced by volatile anesthetics is

mediated by NG2(+) vascular mural cells. Commun Biol *7*, 1519. 10.1038/s42003-024-07200-7.
37. Blaeser, A.S., Sugden, A.U., Zhao, J., Carneiro-Nascimento, S., Shipley, F.B., Carrie, H., Andermann, M.L., and Levy, D. (2022). Trigeminal afferents sense locomotion-related meningeal deformations. Cell Rep *41*, 111648. 10.1016/j.celrep.2022.111648.
38. Mi, X., Chen, A.B., Duarte, D., Carey, E., Taylor, C.R., Braaker, P.N., Bright, M., Almeida, R.G., Lim, J.X., Ruetten, V.M.S., et al. (2025). Fast, accurate, and versatile data analysis platform for the quantification of molecular spatiotemporal signals. Cell *188*, 2794-2809 e2721. 10.1016/j.cell.2025.03.012.
39. Leon Guerrero, P.A., Rasmussen, J.P., and Peterman, E. (2024). Calcium dynamics of skin-resident macrophages during homeostasis and tissue injury. Mol Biol Cell *35*, br26. 10.1091/mbc.E24-09-0420.
40. Paterson, N., and Lammermann, T. (2022). Macrophage network dynamics depend on haptokinesis for optimal local surveillance. Elife *11*. 10.7554/eLife.75354.
41. Behmoaras, J., Mulder, K., Ginhoux, F., and Petretto, E. (2025). The spatial and temporal activation of macrophages during fibrosis. Nature reviews. 10.1038/s41577-025-01186-x.
42. Gao, Y.R., and Drew, P.J. (2016). Effects of Voluntary Locomotion and Calcitonin Gene-Related Peptide on the Dynamics of Single Dural Vessels in Awake Mice. J Neurosci *36*, 2503-2516. 10.1523/JNEUROSCI.3665-15.2016.
43. Pietrobon, D., and Moskowitz, M.A. (2014). Chaos and commotion in the wake of cortical spreading depression and spreading depolarizations. Nat Rev Neurosci *15*, 379-393. 10.1038/nrn3770.
44. Levy, D., and Moskowitz, M.A. (2023). Meningeal Mechanisms and the Migraine Connection. Annual review of neuroscience. 10.1146/annurev-neuro-080422-105509.
45. Schain, A.J., Melo-Carrillo, A., Borsook, D., Grutzendler, J., Strassman, A.M., and Burstein, R. (2018). Activation of pial and dural macrophages and dendritic cells by cortical spreading depression. Ann Neurol *83*, 508-521. 10.1002/ana.25169.
46. Kipnis, J. (2024). The anatomy of brainwashing. Science *385*, 368-370. 10.1126/science.adp1705.
47. Chauhan, A., Sun, Y., Sukumaran, P., Quenum Zangbede, F.O., Jondle, C.N., Sharma, A., Evans, D.L., Chauhan, P., Szlabick, R.E., Aaland, M.O., et al. (2018). M1 Macrophage Polarization Is Dependent on TRPC1-Mediated Calcium Entry. iScience *8*, 85-102. 10.1016/j.isci.2018.09.014.
48. Zhao, J., and Levy, D. (2016). Cortical Spreading Depression Promotes Persistent Mechanical Sensitization of Intracranial Meningeal Afferents: Implications for the Intracranial Mechanosensitivity of Migraine. eNeuro *3*, ENEURO.0287-0216.2016. 10.1523/ENEURO.0287-16.2016.
49. Blaeser, A.S., Zhao, J., Sugden, A.U., Carneiro-Nascimento, S., Andermann, M.L., and Levy, D. (2024). Sensitization of meningeal afferents to locomotion-related meningeal deformations in a migraine model. Elife *12*. 10.7554/eLife.91871.

50. Zhao, J., and Levy, D. (2018). The CGRP receptor antagonist BIBN4096 inhibits prolonged meningeal afferent activation evoked by brief local K(+) stimulation but not cortical spreading depression-induced afferent sensitization. Pain Rep *3*, e632. 10.1097/PR9.0000000000000632.
51. Deng, L., Gillis, J.E., Chiu, I.M., and Kaplan, D.H. (2024). Sensory neurons: An integrated component of innate immunity. Immunity *57*, 815-831. 10.1016/j.immuni.2024.03.008.
52. Jin, X., Morais, A., Sasaki, Y., Zhai, Q., Banerjee, P., Harriott, A., and Ayata, C. (2025). Small-molecule CGRP antagonist atogepant does not affect cortical spreading depression susceptibility in rats. J Headache Pain *26*, 177. 10.1186/s10194-025-02127-8.
53. Rustenhoven, J., and Kipnis, J. (2022). Brain borders at the central stage of neuroimmunology. Nature *612*, 417-429. 10.1038/s41586-022-05474-7.
54. Min, H., O'Neil, S.M., Xu, L., Moseman, E.A., Kurtzberg, J., and Filiano, A.J. (2024). Mural cells interact with macrophages in the dura mater to regulate CNS immune surveillance. J Exp Med *221*. 10.1084/jem.20230326.
55. Dalmau Gasull, A., Glavan, M., Samawar, S.K.R., Kapupara, K., Kelk, J., Rubio, M., Fumagalli, S., Sorokin, L., Vivien, D., and Prinz, M. (2024). The niche matters: origin, function and fate of CNS-associated macrophages during health and disease. Acta Neuropathol *147*, 37. 10.1007/s00401-023-02676-9.
56. Atcha, H., Jairaman, A., Holt, J.R., Meli, V.S., Nagalla, R.R., Veerasubramanian, P.K., Brumm, K.T., Lim, H.E., Othy, S., Cahalan, M.D., et al. (2021). Mechanically activated ion channel Piezo1 modulates macrophage polarization and stiffness sensing. Nat Commun *12*, 3256. 10.1038/s41467-021-23482-5.
57. Tong, L., Hill, R.A., Damisah, E.C., Murray, K.N., Yuan, P., Bordey, A., and Grutzendler, J. (2021). Imaging and optogenetic modulation of vascular mural cells in the live brain. Nature protocols *16*, 472-496. 10.1038/s41596-020-00425-w.
58. Semyanov, A., and Verkhratsky, A. (2021). Astrocytic processes: from tripartite synapses to the active milieu. Trends Neurosci *44*, 781-792. 10.1016/j.tins.2021.07.006.
59. Takano, T., Tian, G.F., Peng, W., Lou, N., Lovatt, D., Hansen, A.J., Kasischke, K.A., and Nedergaard, M. (2007). Cortical spreading depression causes and coincides with tissue hypoxia. Nat Neurosci *10*, 754-762. 10.1038/nn1902.
60. Rosic, B., Dukefoss, D.B., Abjorsbraten, K.S., Tang, W., Jensen, V., Ottersen, O.P., Enger, R., and Nagelhus, E.A. (2019). Aquaporin-4-independent volume dynamics of astroglial endfeet during cortical spreading depression. Glia *67*, 1113-1121. 10.1002/glia.23604.
61. Lu, Y.Z., Nayer, B., Singh, S.K., Alshoubaki, Y.K., Yuan, E., Park, A.J., Maruyama, K., Akira, S., and Martino, M.M. (2024). CGRP sensory neurons promote tissue healing via neutrophils and macrophages. Nature *628*, 604-611. 10.1038/s41586-024-07237-y.
62. Hasegawa, T., Lee, C.Y.C., Hotchen, A.J., Fleming, A., Singh, R., Suzuki, K., Yuzaki, M., Watanabe, M., Birch, M.A., McCaskie, A.W., et al. (2024). Macrophages and nociceptor neurons form a sentinel unit around fenestrated

capillaries to defend the synovium from circulating immune challenge. Nat Immunol *25*, 2270-2283. 10.1038/s41590-024-02011-8.

63. Fattori, V., Zaninelli, T.H., Rasquel-Oliveira, F.S., Heintz, O.K., Jain, A., Sun, L., Seshan, M.L., Peterse, D., Lindholm, A.E., Anchan, R.M., et al. (2024). Nociceptor-to-macrophage communication through CGRP/RAMP1 signaling drives endometriosis-associated pain and lesion growth in mice. Sci Transl Med *16*, eadk8230. 10.1126/scitranslmed.adk8230.

Figure 1

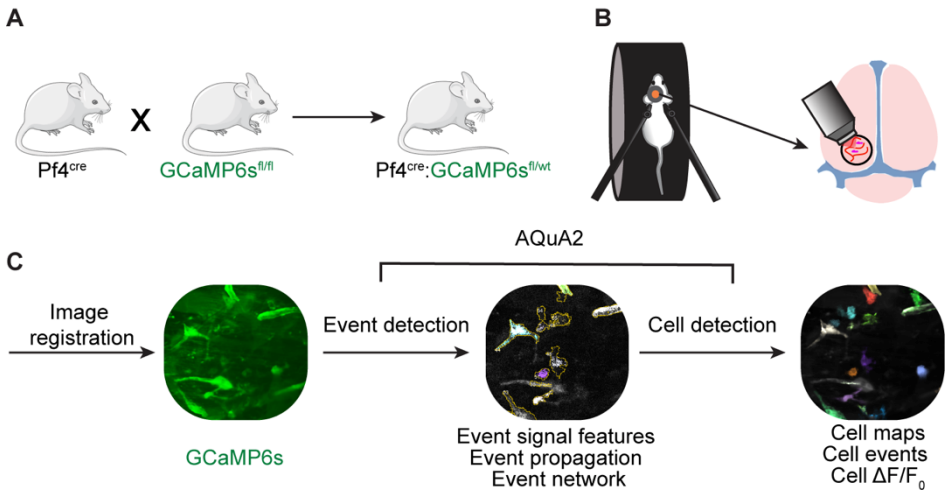

Figure 1. Imaging meningeal macrophage Ca^{2+} activity in awake behaving mice.
(A) $Pf4^{Cre}$:$GCaMP6s^{fl/wt}$ reporter mouse construct for imaging meningeal macrophages Ca^{2+} activity.
(B) Experimental procedure for two-photon imaging of meningeal macrophage Ca^{2+} activity. Following the implantation of a headpost and a cranial window, mice were habituated to head restraint and subjected to two-photon microscopy while head-fixed on a running wheel to study meningeal macrophage Ca^{2+} activity.
(C) Macrophage Ca^{2+} imaging processing pipeline.

Figure 2

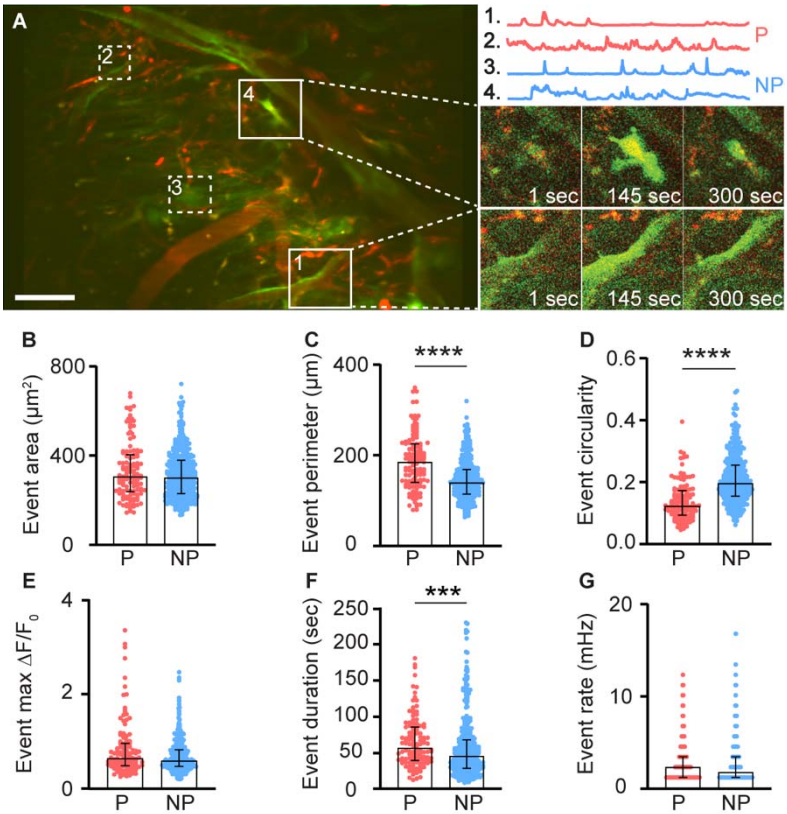

Figure 2. Ca^{2+} activity features of meningeal macrophages at Steady state

(A) Left: Mean projection of an example FOV depicting perivascular (P, red; 1, 2) and non-perivascular (NP, blue; 3, 4) meningeal macrophages (white squares). Scale bar 50 µm. Right: Corresponding macrophages with representative 900-second Ca^{2+} activity traces (top) and their fluorescence signal at selected time points (bottom).

(B-G) AQuA2-based morphological and Ca^{2+} event functional features of perivascular (P=122) and non-perivascular (NP, n=381) meningeal macrophage. (B) Event area, (C) Event perimeter, (D) Event circularity, (E) Event max DF/F_0, (F) Event duration, (G) Event rate.

Data (B-G) represent median ± IQR. ***$p < 0.001$, ****$p < 0.0001$, Mann-Whitney U-test. n=37 fields of view (FOVs) from 7 mice.

Figure 3

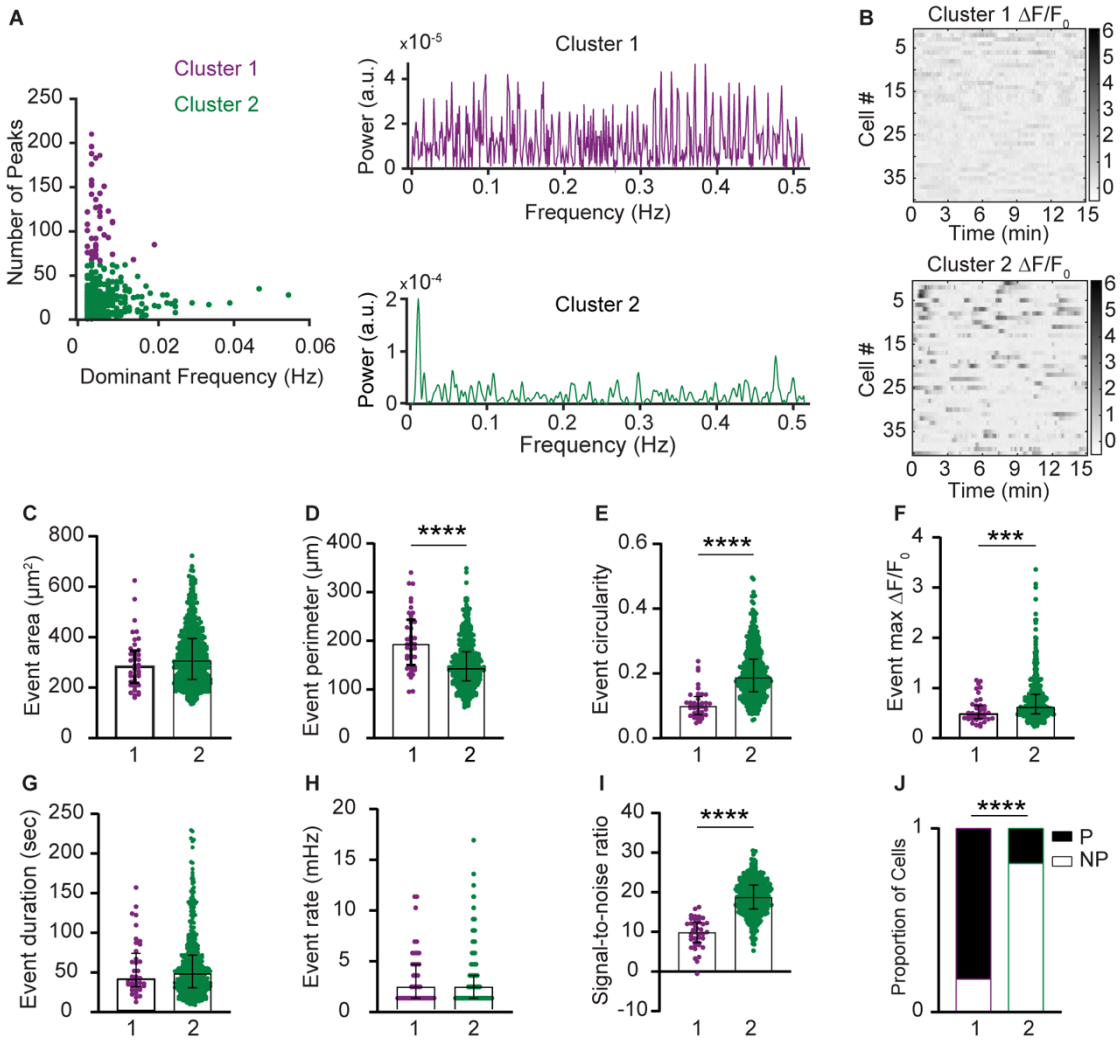

Figure 3. Intracellular Ca^{2+} signal frequency spectra of meningeal macrophage subsets under steady-state

(A) Left: clustering of meningeal macrophage Ca^{2+} activity based on frequency-domain features and peak detection. Cluster 1 (purple, n=40) and Cluster 2 (green, n=463). Right: Power spectrum density (PSD) of Ca^{2+} signals for each cluster.

(B) Example DF/F_0 heatmaps of Cluster 1 and Cluster 2 macrophages.

(C-H) Morphological and Ca^{2+} functional features of Cluster 1 and Cluster 2 macrophages. (C) Event area. (D) Event perimeter (E) Event circularity. (F) Event max DF/F_0. (G) Event duration. (H) Event rate. (I) Signal-to-noise ratio from Clusters 1 and 2**.** (J) Distribution of cell types across clusters.

Data (C-I) represents median ± IQR. ***$p < 0.001$, ****$p < 0.0001$, Mann-Whitney U-test

Data (J) represents the cell proportion. ****$p < 0.0001$, Chi-square test.

Figure 4

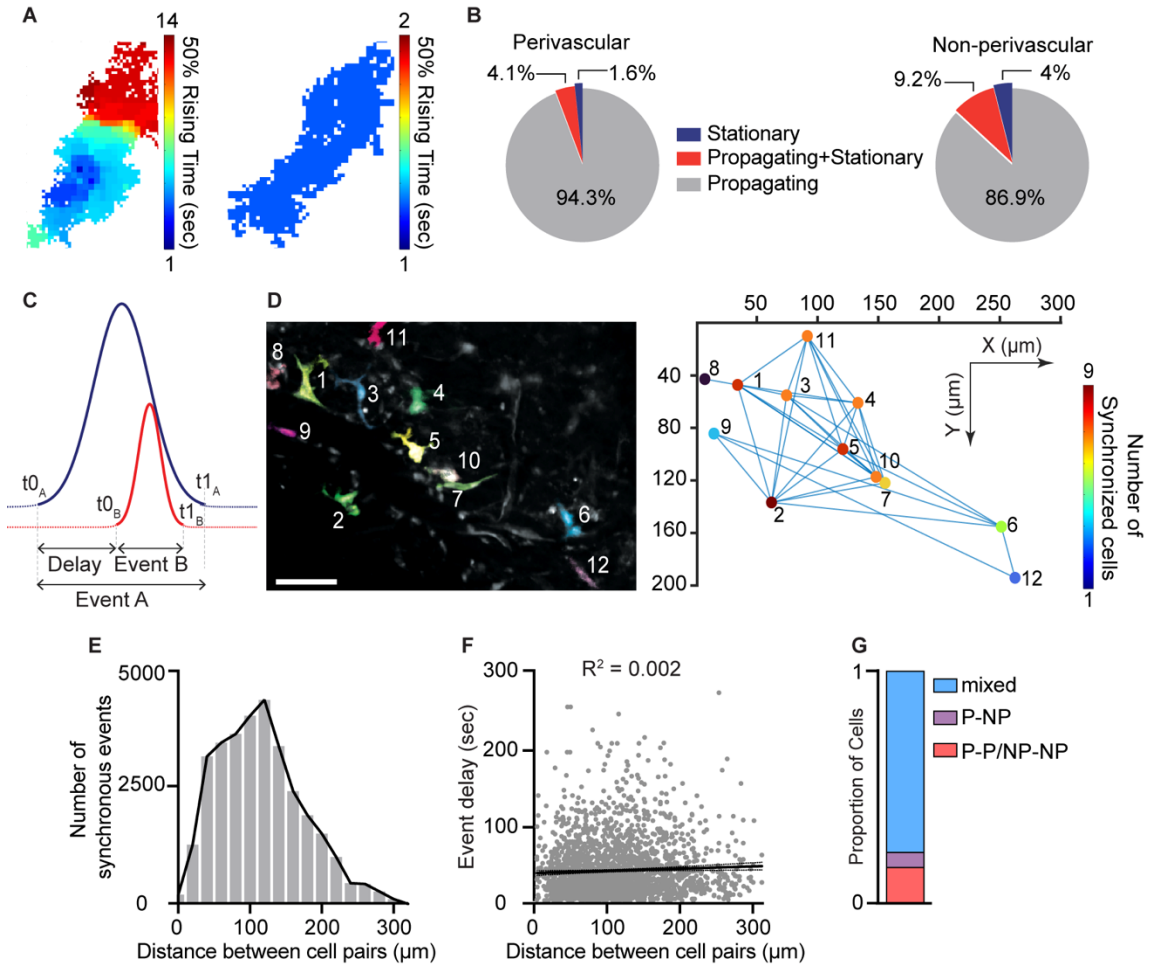

Figure 4. Intracellular propagation and intercellular synchronization of meningeal macrophage Ca^{2+} activity.

(A) Spatial maps of two distinct Ca^{2+} events. Left: propagating Ca^{2+} activity. Right stationary Ca^{2+} activity:

(B) Distribution of event propagation profiles in perivascular and non-perivascular meningeal macrophages.

(C) Schematic analysis paradigm for detecting synchronous Ca^{2+} activity in meningeal macrophages.

(D) Synchronous Ca^{2+} events among meningeal macrophages within a FOV. Left: Mean projection of an example FOV showing Ca^{2+} activity in distinct macrophages (colored/numbered). Scale bar 50 μm. Right: Spatial map of macrophages exhibiting synchronous Ca^{2+} activity. Lines connect macrophages with synchronized Ca^{2+} activity, and colors indicate the extent of Ca^{2+} event synchronization.

(E) Distribution of distances across macrophage pairs showing different numbers of synchronous Ca^{2+} events.

(F) Linear regression showing poor correlation between distances of macrophage with synchronized Ca^{2+} activity and event delay.
(G) Proportion of macrophages exhibiting a specific synchronized interaction (cells interacting only with the same subtype: P-P/NP-NP; cells interacting only with a different subtype: P-NP; mixed (cells interacting with the same and different subtypes).

Figure 5

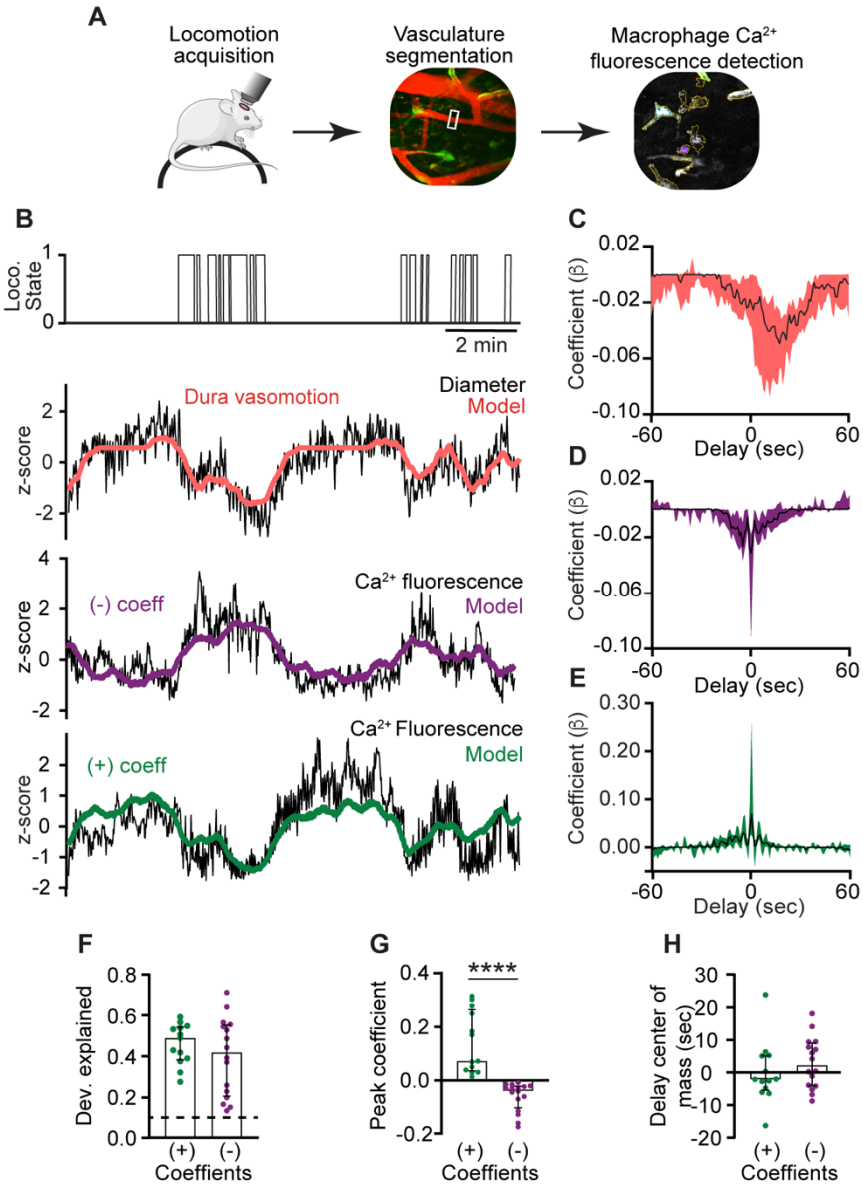

Figure 5. Dural perivascular macrophages Ca^{2+} signals are functionally coupled to behaviorally driven dural vasomotion

(A) Experimental paradigm: Locomotion data were acquired during imaging in awake-behaving mice. Behaviorally-evoked changes in meningeal vessel diameter were obtained using segmentation of vessels labeled with a tracer during macrophage Ca^{2+} and further tested for coupling with Ca^{2+} signals.

(B) Example data of macrophages with Ca^{2+} activity tuned to locomotion-related dural vessel vasomotion. Locomotion bouts (top trace) and dural vessel diameter (black trace) that was well-fit by a GLM (red line) using locomotion state as a predictor. Note vasoconstriction during locomotion, indicating a dural vessel. The two bottom traces

depict the Ca^{2+} signal (black traces) of distinct meningeal macrophages that were well-fit by a GLM using dural vessel diameter as a predictor, showing either a negative coefficient (purple) or a positive coefficient (green).

(C) Temporal profile of dura vessels GLM coefficients averaged across all well-fitted vessels (n=19). Traces represent the median across all well-fit ROIs, with shaded regions indicating IQR.

(D, E) Temporal profiles of GLM coefficient values for macrophages' Ca^{2+} activity averaged across all well-fitted cells (purple, negative coefficient, n=16; green, positive coefficient, n=13). Traces represent the median across all well-fit macrophages, with shaded regions indicating IQR.

(F) The deviance explained (goodness-of-fit estimates) of the vessel diameter data included in the GLM used to predict macrophage Ca^{2+} activity were not statistically different for macrophages showing negative (n=16) and positive (n=13) coefficients, suggesting similar interaction levels.

(G) Comparison of peak positive and negative coefficients of well-fit macrophage calcium activity/vasomotion GLMs.

(H) Center of mass of GLM coefficients indicating that dural vessel diameter changes drive bidirectional changes in fluorescence signal at zero delay.

Data (F-H) are median ± IQR. ****$p<0.0001$ (Mann-Whitney U-test).

Figure 6

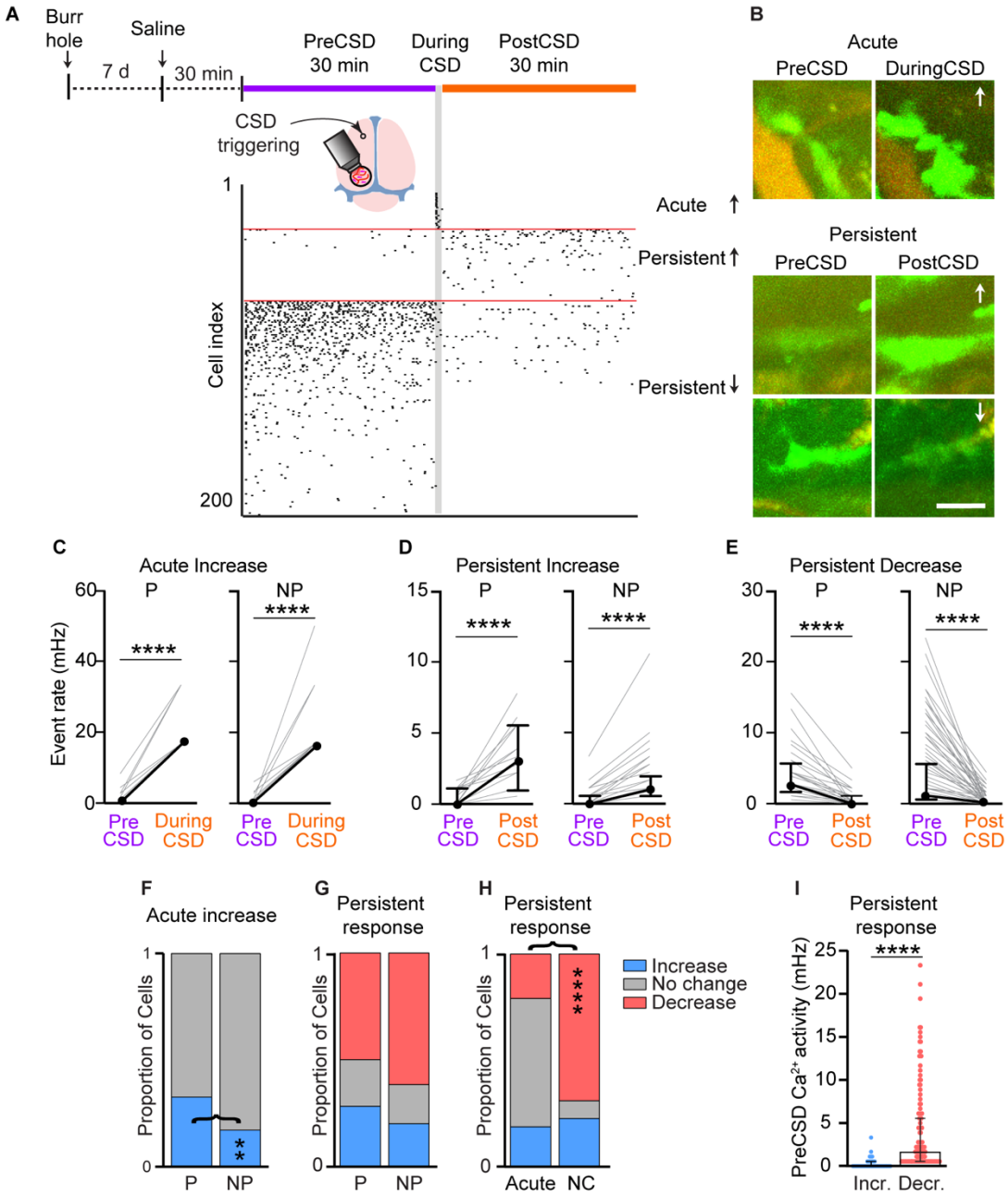

Figure 6. Diverse meningeal macrophage Ca^{2+} responses following cortical spreading depression (CSD).

(A) Experimental setup and example data: (top) A small burr hole was drilled above the frontal cortex 7 days before Ca^{2+} imaging. Mice were pretreated with saline 30 min before imaging baseline macrophage Ca^{2+} activity (30 min, PreCSD). CSD was then

induced with a pin prick, and macrophage Ca^{2+} activity was assessed during CSD (1 min during CSD), and post-CSD (30 min, post-CSD). (Bottom) A raster plot of macrophage Ca^{2+} activity showing the acute and persistent increases and persistent decrease in response to CSD.

(B) Example of macrophage Ca^{2+} fluorescence changes following CSD. Images depict the mean projection over the specific experimental timeline. Arrows indicate an increase or a decrease in Ca^{2+} activity. Scale bar 50 µm.

(C) Individual responses of perivascular (P, n=21) and non-perivascular (NP, n=32) macrophages showing an acute increase in Ca^{2+} activity.

(D) Individual response of P (n=18) and NP (n=37) macrophages exhibiting a persistent increase in Ca^{2+} activity.

(E) Individual responses of P (n=32) and NP (n=114) macrophages showing a persistent decrease in Ca^{2+} activity.

(F) Proportion of P and NP macrophages showing an acute increase in Ca^{2+} activity or no acute change.

(G) Proportion of P and NP macrophages showing a persistent increase, decrease, or no change in Ca^{2+} activity.

(H) Proportion of macrophages displaying distinct persistent responses stratified based on their acute response.

(I) Baseline (PreCSD) Ca^{2+} activity in macrophages exhibiting persistent increased (n=55) or decreased activity (n=146).

Data (C-E) are median ± IQR. ****$p<0.0001$ (Wilcoxon signed rank test). ** Data (F-H) represents the proportion of cells, **$p<0.01$; ****$p<0.0001$ (Chi-square test). Data (I) are median ± IQR. ****$p<0.0001$ (Mann-Whitney U-test).

Figure 7

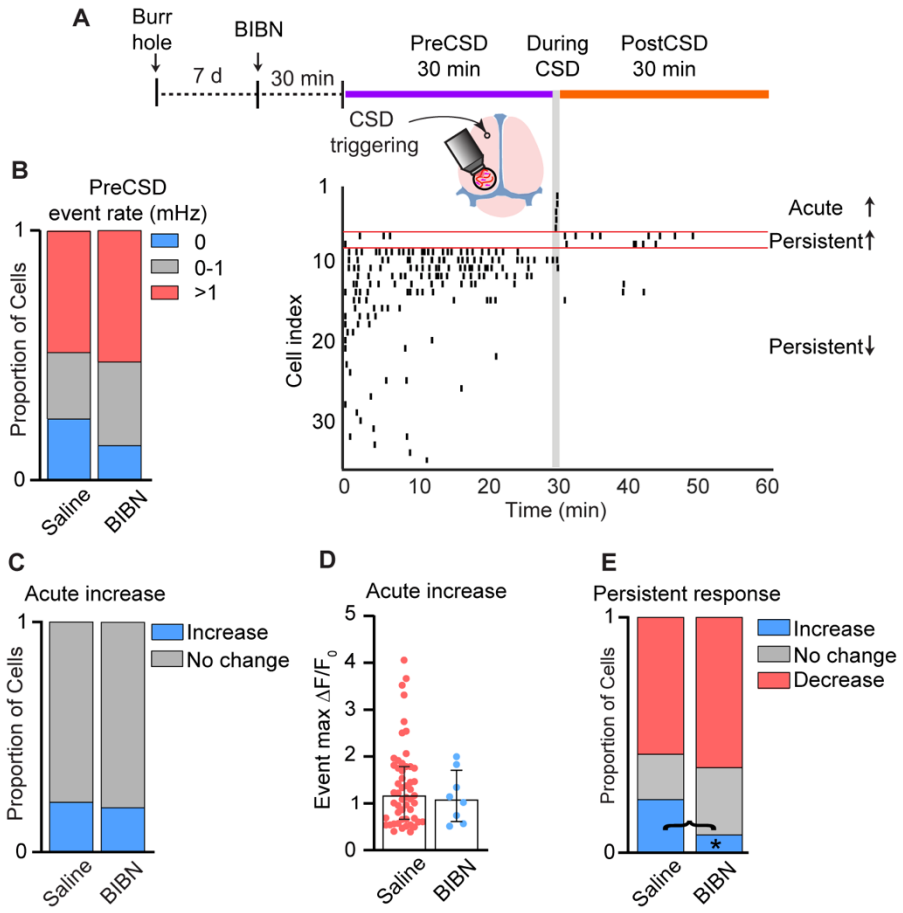

Figure 7. RAMP1 mediates CSD-related persistent increase in meningeal macrophage Ca^{2+} activity.

(A) Experimental setup and example data: (top) A small burr hole was drilled above the frontal cortex 7 days before Ca^{2+} imaging. Mice were pretreated with the RAMP1 antagonist BIBN4096 (BIBN) 30 min before imaging baseline macrophage Ca^{2+} activity (30 min, PreCSD). CSD was then induced with a pin prick, and macrophage Ca^{2+} activity was assessed during CSD (1 min during CSD), and post-CSD (30 min, post-CSD). (Bottom) A raster plot of macrophage Ca^{2+} activity showing the acute and persistent increases and persistent decrease in response to CSD.

(B) RAMP1 inhibition does not affect the baseline (PreCSD) event rate. Data compared between macrophages imaged in saline-treated mice (n=249) and BIBN-treated mice (n=42).

(C) RAMP1 antagonism does not affect the CSD-evoked acute increase in macrophage Ca^{2+}. Proportion of macrophages showing an acute response (increase vs. no change) in saline-treated mice (n=249 cells) and BIBN-treated mice (n=42 cells).

(D) RAMP1 antagonism does not affect the magnitude of the acute macrophage Ca^{2+} signal. Event max DF/F_0 in macrophages showing an acute Ca^{2+} increase in saline-treated mice (n=53 cells) and BIBN-treated mice (n=8 cells).
(E) RAMP1 antagonism distinctly inhibits the persistent increase in macrophage Ca^{2+} activity post CSD. Proportion of macrophages showing persistent increase, persistent decrease, or no persistent change in saline-treated mice (n=249 cells) and BIBN-treated mice (n=42 cells).
Data (B, C, E) represents the proportion of cells. * $p < 0.05$, Fisher's exact test. Data (D) are median ± IQR.

Supplementary video legends:

Video S1. Macrophage Ca^{2+} activity in homeostatic meninges of awake mice
Example two-photon calcium imaging showing activity in perivascular and non-perivascular macrophages (Downsampled movie, frame rate 1Hz).

Video S2. Acute and persistent changes in meningeal macrophage Ca^{2+} Activity in response to CSD.
Example two-photon calcium imaging of baseline and CSD-evoked response. The arrow indicates a macrophage showing an acute activation, the arrowhead depicts a delayed and persistent activation, and the asterisk, a macrophage showing decreased activity. (Downsampled movie, frame rate 1Hz).